Podoplanin Drives Amoeboid Invasion in Canine and Human Mucosal Melanoma

Masahiro Shinada[1], Daiki Kato[1], Tomoki Motegi[2], Masaya Tsuboi[2], Namiko Ikeda[1], Susumu Aoki[1], Takaaki Iguchi[1], Toshio Li[1], Yuka Kodera[1], Ryosuke Ota[1], Yuko Hashimoto[2], Yosuke Takahashi[2], James Chambers[3], Kazuyuki Uchida[3], Yukinari Kato[4,5], Ryohei Nishimura[1], and Takayuki Nakagawa[1]

ABSTRACT

Mucosal melanoma metastasizes at an early stage of the disease in human and dog. We revealed that overexpression of podoplanin in tumor invasion fronts (IF) was related to poor prognosis of dogs with mucosal melanoma. Moreover, podoplanin expressed in canine mucosal melanoma cells promotes proliferation and aggressive amoeboid invasion by activating Rho-associated kinase (ROCK)-myosin light chain 2 (MLC2) signaling. PDPN-ROCK-MLC2 signaling plays a role in cell-cycle arrest and cellular senescence escape as a mechanism for regulating proliferation. Podoplanin induces amoeboid invasion in the IFs of mouse xenografted tumor tissues, similar to canine mucosal melanoma clinical samples. We further identified that podoplanin expression was related to poor prognosis of human patients with mucosal melanoma, and human mucosal melanoma with podoplanin-high expression enriched gene signatures related to amoeboid invasion, similar to canine mucosal melanoma. Overall, we propose that podoplanin promotes canine and human mucosal melanoma metastasis by inducing aggressive amoeboid invasion and naturally occurring canine mucosal melanoma can be a novel research model for podoplanin expressing human mucosal melanoma.

Implications: Podoplanin could be a new therapeutic target to restrict the metastatic dissemination of canine and human mucosal melanoma.

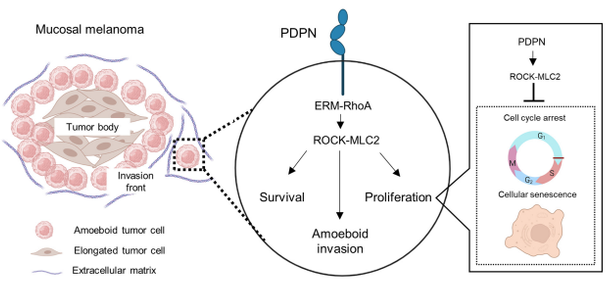

Introduction

Human mucosal melanoma is the most aggressive subtype of melanoma, and most patients develop an incurable metastatic disease, irrespective of surgical removal (1). There is little effective systemic therapy for human mucosal melanoma, and patients with mucosal melanoma have worse prognoses than those with common cutaneous melanoma, with a 5-year survival rate of 25% and 90%, respectively. Therefore, it is crucial to develop a therapeutic strategy to restrict the metastasis of human mucosal melanoma (1–4). However, human mucosal melanoma research on the molecular mechanisms of tumor progression, therapeutic targets, and biomarkers has not advanced owing to its rarity, accounting for only 1% to 2% of all melanomas, with an incidence of 2.2 per 1,000,000 persons/year (5–7).

Canine melanoma is a frequent tumor in dogs, reaching 100,000 diagnoses per year in the United States (8–10). In contrast to human melanoma, approximately 60% to 70% of canine melanomas originate from the gingiva of oral cavities and are classified as mucosal melanomas (8). Generally, complete surgical removal is performed to manage the local tumor; however, similar to human mucosal melanoma, local recurrence and distant metastasis frequently occur (8, 10). Notably, naturally occurring canine mucosal melanomas share many similarities with human counterpart, including genetic mutations, histopathologic features, and clinical behavior (8, 11–13). Therefore, naturally occurring canine mucosal melanoma could be a novel research model for human mucosal melanoma (14–16).

Canine mucosal melanoma cells were recently found to express podoplanin, a small transmembrane mucin-like glycoprotein (17, 18). Podoplanin-targeting cytotoxic antibody therapy has exhibited antitumor efficacy in dogs with mucosal melanoma (17). Overexpression of podoplanin has been observed in human epithelial tumors, and the intracellular domain of overexpressed podoplanin binds to the exrin/radixin/moesin (ERM), which activates RhoA, a Rho-GTPase family protein (19–22). Podoplanin expression is related to the frequency of metastasis and poor prognosis of human patients with squamous cell carcinoma (SCC; refs. 23, 24). A previous report showed that podoplanin promotes tumor growth and migration of human and murine cutaneous melanoma cells (25). Furthermore, the extracellular domain of podoplanin has been shown to bind to platelets to promote tumor growth and pulmonary metastasis of human cutaneous melanoma cells (26). However, the intercellular signaling of podoplanin in canine and human mucosal melanoma cells has not been explored.

Invasive human cutaneous melanoma cells have high cellular plasticity, shifting from the mesenchymal to the amoeboid mode of

[1]Laboratory of Veterinary Surgery, Graduate School of Agricultural and Life Sciences, The University of Tokyo, Tokyo, Japan. [2]Veterinary Medical Center, The University of Tokyo, Tokyo, Japan. [3]Laboratory of Veterinary Pathology, Graduate School of Agricultural and Life Sciences, The University of Tokyo, Tokyo, Japan. [4]Department of Antibody Drug Development, Tohoku University Graduate School of Medicine, Miyagi, Japan. [5]Department of Molecular Pharmacology, Tohoku University Graduate School of Medicine, Miyagi, Japan.

Corresponding Author: Daiki Kato, Laboratory of Veterinary Surgery, Graduate School of Agricultural and Life Sciences, The University of Tokyo, 1-1-1 Yayoi, Bunkyo-Ku, Tokyo 113-8657, Japan. E-mail: adk@g.ecc.u-tokyo.ac.jp

Mol Cancer Res 2023;21:1205–19

doi: 10.1158/1541-7786.MCR-22-0929

motility to aggressively invade the extracellular matrix (ECM), a process referred to as amoeboid invasion (27–31). Amoeboid-invading cells are often enriched in the tumor invasion fronts (IF) of primary human cutaneous melanoma compared with the tumor bodies (TB) and possess high proliferative, migratory, invasive, and metastasis colonizing characteristics (27–31). Therefore, amoeboid invasion is considered a leading driver of the many steps required for the metastatic success of human cutaneous melanoma, including separating from the primary tumor nests, invasion into blood veins and regional lymph nodes, and colonization of metastatic nests (27–31). Previously, podoplanin was reported to promote amoeboid invasion of murine cutaneous melanoma cells (32), thus we hypothesized that podoplanin drives amoeboid invasion in canine and human mucosal melanoma.

Our results show that podoplanin overexpressed in canine mucosal melanoma IFs drives amoeboid invasion via Rho-associated kinase (ROCK)-myosin right chain 2 (MLC2) signaling. Podoplanin expressing amoeboid invading canine mucosal melanoma cells show highly proliferative and invasive characteristics, and escape from cell-cycle arrest and cellular senescence by activating ROCK–MLC2 signaling. Moreover, human mucosal melanoma with podoplanin-high expression enriched gene signatures related to amoeboid invasion and showed poor prognosis, similar to canine mucosal melanoma.

Materials and Methods

Cell culture

Canine melanoma cell lines, CMM2 and CMM12, were established in our laboratory, as previously reported (18, 33, 34). CMM2 cells were cultured in RPMI1640 (FUJIFILM Wako) supplemented with 10% heat-inactivated FBS (Serana Europe GmbH) and 5 mg/L gentamicin (Sigma-Aldrich Corp.). CMM12 cells were cultured in DMEM/Ham F-12 medium (FUJIFILM Wako) with 10% FBS, 100 U/mL penicillin, and 100 μg/mL streptomycin (FUJIFILM Wako). Cells were maintained at 37°C in a humidified atmosphere containing 5% CO_2. Podoplanin knocked out (PDPN-KO) cells were generated using CRISPR/Cas9. The CRISPR/Cas9 vector was the pGuide-it-ZsGreen1 vector (Takara Bio Inc.). Plasmid DNA was transfected using Xfect transfection reagent (Takara Bio Inc.). The sequence of the single-guide RNA (sgRNA) targeting canine podoplanin was ACCGGGCAGCCGACGAGATG. To generate podoplanin-overexpressed PDPN-KO cells (PDPN-KO-OE), CMM2 PDPN-KO#2 and CMM12 PDPN-KO#2 cells were transfected with the lentivirus vector plasmid pCSII-CMV-MCS (RIKEN BRC DNA Bank) encoding canine podoplanin cDNA (NM_001003220.1). Transfected cells were selected with puromycin (FUJIFILM Wako).

Inhibitors

ROCK (Fasudil, GSK269962A, and Y-27632) and myosin II inhibitors [(−)-blebbistatin] were purchased from Selleck Chemicals. Concentrations used unless otherwise stated were: 100 and 200 μmol/L Fasudil, 1 and 2 μmol/L GSK269962A, 100 and 200 μmol/L Y-27632, and 30 and 60 μmol/L (−)-blebbistatin for CMM2 and CMM12, respectively. Unless otherwise stated, the treatment time was 24 hours. Information of antibodies and reagents are described in Supplementary Data.

IHC

IHC was performed as described previously (18) and detailed methods are described in Supplementary File. The IFs and TBs were evaluated separately. The IFs were defined as melanoma cells with at least 50% contact with the matrix (29). Quantitative scores of 0, 1, 2, 3, 4, or 5 were assigned when 0, 1 to 10, 11 to 30, 31 to 50, 51 to 80, or 81% to 100% of the melanoma cells were podoplanin positive, respectively. The staining intensity of podoplanin was rated on a scale of 0 to 3 where 0 = negative, 1 = weak, 2 = moderate, and 3 = strong. Raw data were converted to IHC scores by multiplying the quantity and staining intensity scores (24). An IHC score above the median value was considered indicative of high podoplanin expression. Morphologic analysis of tumor tissues was performed using hematoxylin and eosin (H&E)-stained sections as described previously. Cell shape was graded from 0 to 3 (0 = round, 1 = ovoid, 2 = elongated, and 3 = spindly), and a score was assigned as follows: cell shape score = [(percentage of cells; % shape 0 × 0) + (% shape 1×1) + (% shape 2×2) + (% shape 3×3)], with values ranging from 0 (all cells round) to 300 (all cells spindle). For phosphor-MLC2 staining, three different thresholds were applied according to the intensity scores (0, 1, 2, and 3), and a score was assigned as follows: phosphor-MLC2 score = [percentage of cells; % intensity 0×0) + (% intensity 1×1) + (% intensity 2×2) + (% intensity 3×3)], with values ranging from 0 (no phosphor-MLC2 expression) to 300 (all cells strongly expressed phosphor-MLC2). All evaluations were performed using blinding clinicopathologic features.

Cell proliferation assay

Cells were stained with trypan blue. The cells were manually counted, and the live cell count (unstained cells) was determined.

Annexin V/propidium iodide FACS

Detection of apoptosis cells was performed as described previously (18) and detailed methods are described in Supplementary Data.

Cell-cycle analysis

Cell-cycle analysis was performed as previously described (18) and detailed methods are described in Supplementary Data.

Wound healing assay

A scratch wound was created in the cell monolayer using a 1,000-μL pipette tip and washed with culture medium to remove floating cells. The migrated areas were manually calculated using ImageJ software (https://imagej.nih.gov/ij; ref. 35).

Transwell invasion assay

Transwell invasion assay was performed as described previously (18) and detailed methods are described in Supplementary Data.

mRNA sequencing

Total RNA was extracted using the RNeasy Mini Kit (Qiagen) according to the manufacturer's protocol. mRNA sequencing (mRNA-seq) was performed using NovaSeq 6000/PE150. Raw sequence reads were trimmed to remove adaptors and quality control using fastp (version. 0.2.0; ref. 36). Mapping and transcript abundance estimating were performed as in a previous report. These gene raw count data were normalized by transcripts per kilobase million (TPM; ref. 37). Gene expression differences between control and PDPN-KO cells were calculated using TPM normalized expression scores, and genes with fold change > 1.2 or < 0.83 (Ctrl KO#1 and KO#2) were defined as differentially expressed genes (DEG). Genes whose TPM in control cells was < 1.0 were excluded from the analyses. Gene ontology (GO) term enrichment and Kyoto encyclopedia of genes and genomes (KEGG) pathway analyses were performed using DAVID (ver. DAVID Knowledgebase v2022q1).

Western blot analysis

Western blot analysis was performed as described previously (18). Briefly, cells were lysed in RIPA buffer supplemented with 10 mmol/L NaF, 2 mmol/L Na_3VO_4, and a complete Mini Protease Inhibitor Cocktail (Roche Diagnostics). After blocking with blocking buffer for 1 hour, primary antibodies were incubated overnight at 4°C. The membranes were then incubated with horseradish peroxidase (HRP)-conjugated antibodies. Membranes were developed using the ECL Prime western blotting Detection System (GE Healthcare), and luminescence was captured and quantified using an imaging system (ChemiDoc Image Lab, Bio-Rad Laboratories).

RhoA-GTP pulldown assay

RhoA-GTP pulldown assay was performed using the RhoA Pull-Down Activation Assay Biochem Kit, according to the manufacturer's protocol (#BK-036, Cytoskeleton, Inc.). Briefly, cells were lysed RIPA buffer. Proteins (50 μg) were incubated with 15 μg glutathione S-transferase (GST)-conjugated Rhotekin RBD beads for 1 hour. RhoA expression was detected using immunoblotting. HRP-conjugated anti-mouse IgM antibody (Abcam) was used as the secondary antibody.

Cell culture on thick layers of collagen I

Collagen I mix (Cellmatrix Type I-A, Nitta Gelatin) was prepared according to the manufacturer's protocol with a final concentration of 1.0 mg/mL. After polymerization (4 hours), cells were seeded on top of collagen in medium containing 10% FBS, allowed to adhere for 24 hours and media was changed to 1% FBS with or without inhibitors. Cell morphology was analyzed using ImageJ software by manually drawing around the cells. The roundness index was calculated as $4 \times \text{area} \times \pi/\text{perimeter}^2$.

Gel contraction assay

Plates were incubated with 1% BSA in PBS for 1 hour. After washing the plates with PBS, cells were embedded in collagen I mix (Cellmatrix Type I-A) with a final concentration of 1.8 mg/mL. The gel was incubated at 37°C for 1 hour, and the medium, with or without inhibitors, was added. A pipette tip was used to loosen the gel from the tissue culture vessel and incubated for 48 hours. The plate image was scanned using ChemiDoc, and the percentage of gel contraction was calculated using the ImageJ software.

Time-lapse imaging

Cells were seeded on 24-well plates, and images were captured for 8 hours at 30 minutes intervals using a microscope (BZ-X810; Keyence).

Senescence-associated β-galactosidase stain

Senescence-associated beta-galactosidase (SA-β-GAL) staining was performed using the Senescence β-Galactosidase Staining Kit (#9860, Cell Signaling Technology) according to the manufacturer's protocol. Three random fields (×200) were assessed in each well.

Animal study

BALB/c-nu/nu mice (BALB/cSlc-nu/nu, 6-week-old female, Japan SLC) and NOD/Shi-scid, IL-2RγKO (NOG) mice (6- to 12-week-old females, Central Institute for Experimental Animals) were maintained under specific pathogen-free conditions at 24 ± 1°C, 40% to 70% humidity, and a 12-hour light–dark cycle throughout all the experiments. A total of 2.5×10^6 CMM2 and PDPN-KO cells derived from CMM2 cells were subcutaneously injected into nude mice. A total of 1×10^7 CMM12 and PDPN-KO cells derived from CMM12 cells were subcutaneously injected into NOG mice. Tumor volumes were measured every 2 to 3 days. Tumor volume was calculated using the following approximation formula: tumor volume = $1/2 \times (\text{major radius}) \times (\text{minor radius})^2$. The study protocol was approved by the University of Tokyo Animal Care and Use Committee (approval numbers P19–126H03 and P19–124).

BALB/c-nu/nu mice (BALB/cSlc-nu/nu, 11-week-old female, Japan SLC) were used for lung metastasis assay. A total of 1×10^6 CMM2 and PDPN-KO cells derived from CMM2 cells were intravenously injected into the mice. Then, 25 days after tumor cell injection, the mice were euthanized, lung tissues were collected, and the number of metastatic foci was counted.

GO terms enrichment analysis and gene-set enrichment analysis for public datasets

Information of the public datasets used is described in Supplementary Data. Gene expression differences between high and low podoplanin expression tumors were evaluated using the Student *t* test. Significantly higher expressed genes in tumors with high podoplanin expression were defined as DEGs. When the total sample number was >10, the statistical significance criterion was $P < 0.01$; when the total sample number was <10, the criterion was $P < 0.05$.

Gene sets were downloaded and analyzed using the GSEA software (ver.4.2.2; ref. 38). The melanoma invasion gene set (39) and mesenchymal amoeboid transition gene set (40) were referred to in previous studies. Gene-set enrichment analysis (GSEA) was performed using the following settings: permutations, 1,000; permutation type, gene set; and metric for ranking genes, *t* test. Mucosal melanoma samples from dogs and humans were divided into high and low podoplanin expression groups based on median podoplanin expression. To perform GSEA using canine samples, all ensemble gene IDs were converted from *Canis familiaris* to *Homo sapiens* using R software (ver. 4.2.0, R Development Core Team, 2019) with the "biomaRt" package (ver. 2.44.4). Significantly enriched gene sets in podoplanin -high expression versus podoplanin -low expression samples were considered according to nominal $P < 0.05$. Mesenchymal amoeboid transition gene expression in human and canine mucosal melanoma tissues was evaluated according to a previous report (40). Genes whose average expression in high- podoplanin–expressing tissues was more than 1.2-fold compared with those of low podoplanin–expressing tissues were selected and heat map images were generated.

Statistical analysis

R software was used for statistical analyses, and used packages were described in Supplementary Data. Student *t* test and χ^2 test were used for two group comparisons. Dunnett and one-way ANOVA with Tukey–Kramer tests were used for multigroup comparisons. Survival curves were estimated by the Kaplan–Meier method and differences were estimated by the log rank test. In figure legends, "*n*" indicates the number of biologic replicates. $P < 0.05$ was defined as significant.

Data availability

mRNA-seq data of control and PDPN-KO canine mucosal melanoma cells are available in the Genome Expression Omnibus with accession number: GSE208269.

Supplementary experimental procedures

Other detailed experimental procedures are described in Supplementary Materials and Methods.

Results

PDPN is overexpressed in canine mucosal melanoma cells in the tumor IFs and associated with poor prognosis in dogs

To evaluate the relationship between podoplanin expression and clinicopathologic features of dogs with mucosal melanoma, IHC for podoplanin was performed in 43 canine oral mucosal melanoma tissues (Supplementary Table S1) and 6 normal gingival mucosa tissues. Podoplanin was expressed in 88% (38/43) of the canine mucosal melanoma tissues, whereas no podoplanin expression was detected in the normal gingival mucosa epithelium (**Fig. 1A–C**). Podoplanin-positive cells were confirmed as canine mucosal melanoma cells by double staining with podoplanin and SOX10—canine mucosal melanoma markers (ref. 41; Supplementary Fig. S1A). The positivity and intensity of podoplanin expression were higher in the IFs of canine mucosal melanoma tissues than in the TBs (mean positivity 42% vs. 29%, mean intensity score 2.0 vs. 0.8, respectively; **Fig. 1A–C**). High podoplanin expression in the IFs was significantly associated with reduced progression-free survival (PFS) and overall survival (OS) rates in dogs with mucosal melanoma, while high podoplanin expression in the TBs was not significantly associated with PFS and OS rates (**Fig. 1D**; Supplementary Table S2; Supplementary Fig. S1B). Overall, podoplanin overexpressed in canine mucosal melanoma IFs was associated with a poor prognosis in dogs.

Podoplanin regulates canine mucosal melanoma proliferation, survival, migration, and invasion

To evaluate the functions of podoplanin in canine mucosal melanoma, PDPN-KO cells were generated using CRISPR/Cas9 technology from two canine mucosal melanoma cell lines (CMM2 and CMM12; Supplementary Fig. S2A and S2B). PDPN-KO cells exhibited slow growth and an increase in apoptotic cells with downregulation of the antiapoptotic protein; BCL-2 and upregulation of the proapoptotic protein; BAX compared with control cells (**Fig. 2A** and **B**; Supplementary Fig. S2C and S2D). In addition, PDPN-KO cells showed lower migration across two-dimensional (2D) surfaces and lower invasiveness in a three-dimensional (3D) ECM compared with control cells (**Fig. 2C** and **D**; Supplementary Fig. S2E).

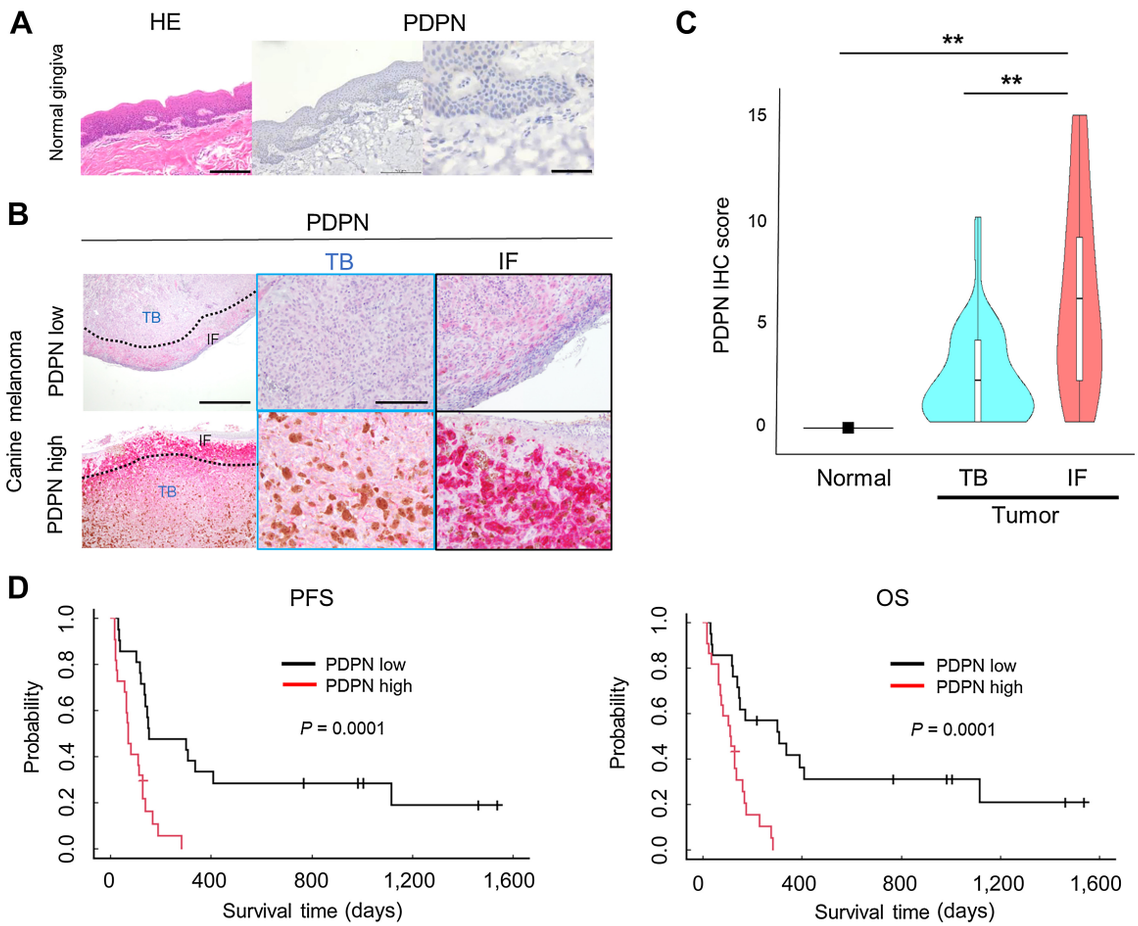

Figure 1.

Podoplanin overexpression in the IFs is associated with poor prognosis in dogs with mucosal melanoma. **A–B,** Podoplanin expression in normal gingival mucosal tissues and in the TBs and IFs of canine mucosal melanoma tissues. Podoplanin was stained with alkaline phosphatase, and podoplanin-positive cells were stained red. Scale bars, 200 μm (top left), 500 μm (bottom left) and 100 μm (top right and bottom middle). **C,** IHC scores of podoplanin expression in normal tissues ($n = 6$), the TBs, and IFs from canine mucosal melanoma tissues ($n = 43$). One-way ANOVA with Tukey–Kramer test. **D,** Kaplan–Meier survival curves for PFS: left and OS: right of dogs with mucosal melanoma above and below the median IHC score of PDPN expression in the IFs. Log-rank test. *, $P < 0.05$,; **, $P < 0.01$.

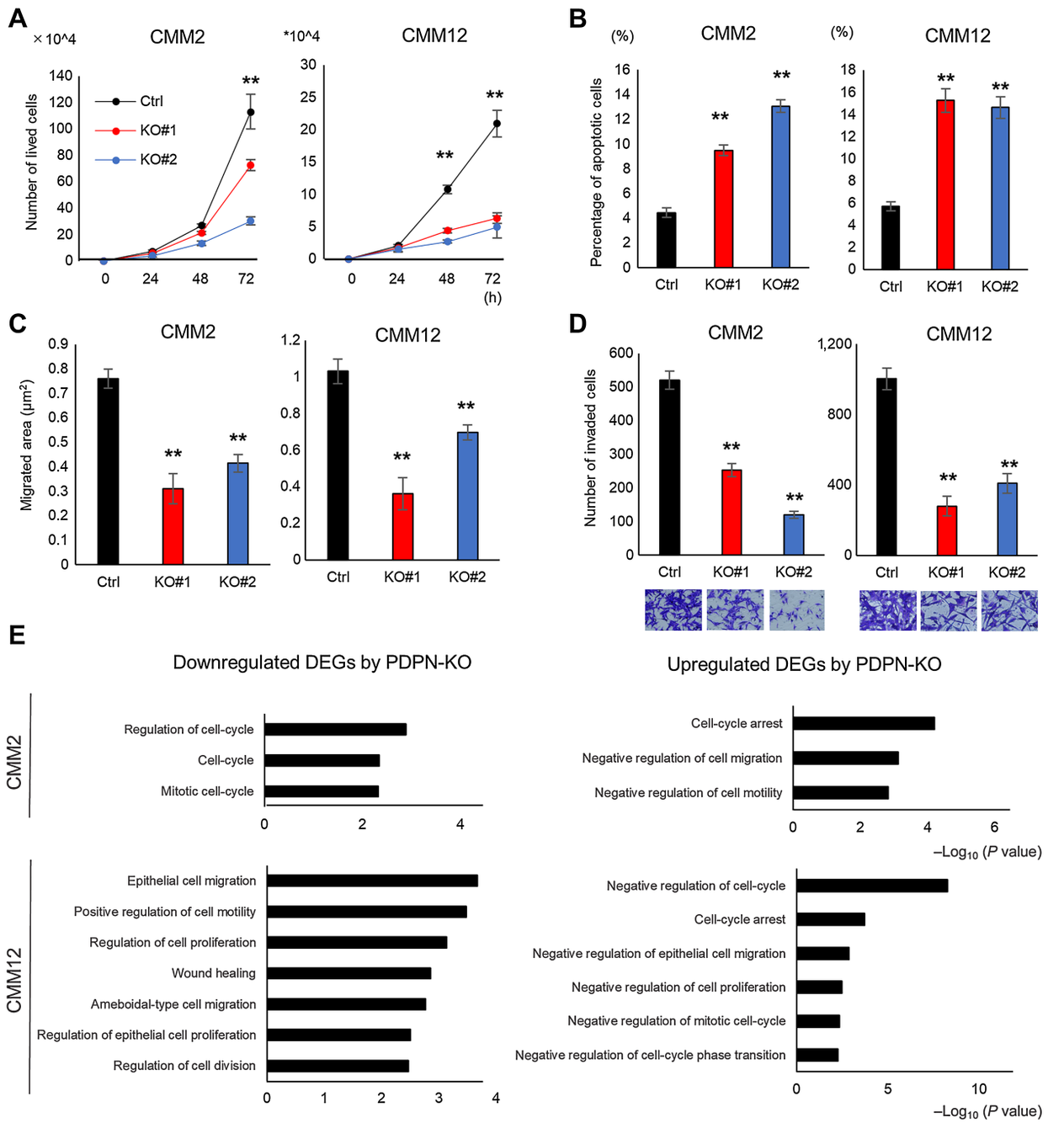

Figure 2.

Podoplanin regulates canine mucosal melanoma proliferation, survival, migration, and invasion. **A,** Number of live cells at 24, 48, and 72 hours after seeding ($n = 3$). **B,** Percentage of annexin V–positive apoptotic cells analyzed by flow cytometry analysis ($n = 3$). **C,** Migrated areas at 8 or 16 hours after wounding ($n = 3$). **D,** Number of invaded cells at 24 hours after cell seeding ($n = 3$). Representative images of wells are shown under the graphs. Graphs show mean ± SD. Dunnett test: *, $P < 0.05$; **, $P < 0.01$. Ctrl: control, KO#1: PDPN-KO cell line 1, KO#2: PDPN-KO cell line 2. **E,** Enriched GO terms in DEGs altered by podoplanin-KO. The x axis indicates the $-\log_{10}$ P value.

Furthermore, DEGs in response to PDPN-KO were detected using mRNA-seq. A total of 560 and 1,132 genes were downregulated and upregulated in the PDPN-KO CMM2 cells, respectively. In addition, 1,726 and 1,122 genes were downregulated and upregulated in the PDPN-KO CMM12 cells, respectively (Supplementary Fig. S2F). In control cells, genes related to cell proliferation and cell-cycle were enriched compared with PDPN-KO cells, whereas genes related to the negative regulation of cell proliferation, cell cycle, and cell motility

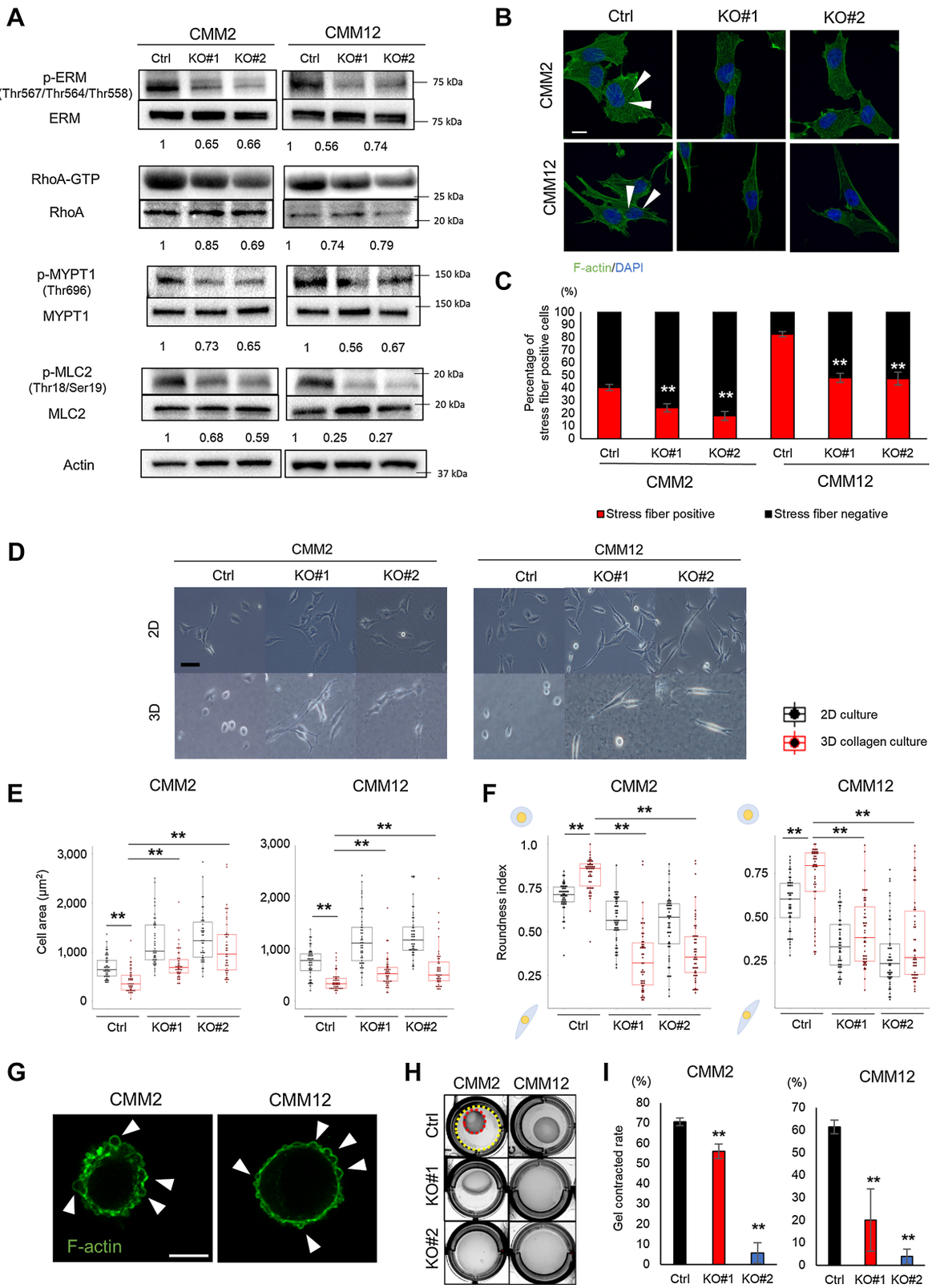

were enriched in PDPN-KO cells (**Fig. 2E**). These results suggest that podoplanin promoted proliferation, survival, migration, and invasion of canine mucosal melanoma cells.

Podoplanin regulates amoeboid invasion features via ROCK-MLC2 signaling

Podoplanin was reported to active ERM and RhoA (20); thus, we evaluated their activation status. PDPN-KO cells exhibited lower ERM phosphorylation and RhoA-GTPase expression, an active form of RhoA, than those of control cells (**Fig. 3A**). Furthermore, PDPN-KO cells exhibited lower myosin phosphatase targeting subunit 1 (MYPT1) and MLC2 phosphorylation, which are ROCK-targeting proteins, than control cells (**Fig. 3A**). The number of cells with cytoplasmic stress fibers was significantly decreased in PDPN-KO cells (**Fig. 3B** and **C**). mRNA-seq also showed an upregulation of ROCK/cytoskeleton-related genes in control cells compared with PDPN-KO cells (Supplementary Fig. S3A).

We explored the morphologic alterations induced by PDPN-KO (27–31). Under 3D collagen culture conditions, control cells displayed a reduction in cell size and an increase in the number of rounded cells compared with 2D culture conditions (**Fig. 3D–F**). The size of the PDPN-KO cells was significantly larger than that of the control cells, and PDPN-KO decreased the number of rounded cells under 3D collagen culture conditions (**Fig. 3D–F**). Controls cells showed membrane blebs under 3D collagen culture conditions (**Fig. 3G**). We then evaluated actomyosin contractile function and found that the contraction rate of embedded PDPN-KO cells was significantly lower than that of control cells (**Fig. 3H** and **I**). Control cells showed lower adhesive capacity compared with PDPN-KO cells (Supplementary Fig. S3B). In addition, a previous report showed that podoplanin regulates proliferation of fibroblasts in a mechanically sensitive mechanism (42). The proliferation of control cells cultured on noncollagen coated dishes (stiffness condition) was increased compared with that of cells cultured on collagen thick layer dish (soft condition; Supplementary Fig. S3C, left), and the changes were dependent on podoplanin expression (Supplementary Fig. S3C, right). Overall, podoplanin in canine mucosal melanoma cells activated ROCK-MLC2 signaling to drive high levels of actomyosin contraction which is necessary for amoeboid invasion.

Loss of podoplanin leads to cell-cycle arrest and cellular senescence

To elucidate the underlying mechanism of PDPN-mediated cell proliferation, a cell-cycle analysis was performed, and the percentage of cells in the S-phase cell-cycle was significantly decreased in PDPN-KO cells (**Fig. 4A**). mRNA-seq of PDPN-KO cells showed an increased gene expression of cyclin-dependent kinase inhibitor (CDKi) compared with control cells (Supplementary Fig. S4A). However, PDPN-KO did not induce a common change in the expression of cyclin and cyclin-dependent kinase genes. A significant upregulation of CDKi mRNA, and p21 and p27 proteins in PDPN-KO cells was confirmed (Supplementary Fig. S4B and S4C). These results indicate that PDPN promotes cell-cycle S-phase entry to support proliferation.

Interestingly, the number of cells with over 4N DNA (G_2–M phase cells) was significantly increased in PDPN-KO cells (**Fig. 4A**). Furthermore, PDPN-KO cells displayed a significant increase in the number of multi-nuclei cells that arise due to cytokinesis failure (43); consequently, cytokinesis failure was frequently observed during the proliferation of PDPN-KO cells (**Fig. 4B** and **C**). These results suggest that the increase of multi-nuclei PDPN-KO cells was due to cytokinesis failure. In addition, SA-β-GAL stain-positive cells were significantly increased among the PDPN-KO cells (**Fig. 4D** and **E**) with upregulated p21 expression in PDPN-KO cells (Supplementary Fig. S4C). p21 expression was upregulated in the nuclei of cytokinesis-failed PDPN-KO cells compared with control cells with a single nucleus (Supplementary Fig. S4D). SA-β-GAL staining intensity and positivity in cytokinesis-failed cells were higher in multi-nuclei PDPN-KO cells than in the control mono nuclear cells (Supplementary Fig. S4E). Genes associated with cellular senescence pathway were enriched in DEGs induced by PDPN-KO (Supplementary Fig. S4F and S4G). Overall, PDPN-KO induced cytokinesis failure in canine mucosal melanoma cells, resulting in cellular senescence.

ROCK inhibition suppresses cell proliferation, migration, and senescence

Next, we pharmacologically inhibited ROCK-MLC2 signaling on canine mucosal melanoma cells to confirm that the loss of ROCK-MLC2 signaling caused cell phenotype modifications in PDPN-KO cells. In inhibitory experiments on canine mucosal melanoma cells, ROCK and myosin II inhibition resulted in a dose-dependent reduction of cell proliferation (Supplementary Fig. S5A and S5B), an increase of the proportion of apoptotic cells, and suppressions of migratory and invasive capacities (Supplementary Fig. S5C–S5F). Moreover, ROCK and myosin II inhibition suppressed stress fiber formation, increased cell area, decreased the number of rounded cells, and reduced gel contractile capacities (**Fig. 5A–C**; Supplementary Fig. S6A–S6C). The percentage of cells in the S-phase cell-cycle was significantly reduced, and the percentage of cells with over 4N DNA was significantly increased by ROCK and myosin II inhibition (Supplementary Fig. S7A). The proportion of multi-nuclei cytokinesis-failure cells and the number of SA-βGAL stain-positive cells increased with the upregulation of p21 expression by ROCK and myosin II inhibition (Supplementary Fig. S7B–S7E). Moreover, restoring podoplanin expression in PDPN-KO cells (KO#2) rescued the podoplanin induced features of amoeboid invasion including the decrease of cell proliferation, p-MLC2 suppression, increase of cell size, and change to an elongated cell shape (**Fig. 5D–H**; Supplementary Fig. S7F). Overall, the inhibition of ROCK-MLC2 signaling in canine

Figure 3.

Podoplanin regulates amoeboid invasion features via ROCK-MLC2 signaling. **A,** Immunoblots of p-ERM, RhoA-GTP, p-MYPT1, and p-MLC2. Levels of phospho-protein expression were calculated after correction to total levels of the relevant protein expression and are indicated under the immunoblot images of each total protein. **B,** Confocal images of phalloidin and 4′,6-diamidino-2-phenylindole (DAPI) staining. Arrowheads show stress fibers in the cytoplasmic regions. Scale bar, 10 μm. **C,** Percentage of stress fiber–positive and-negative cells ($n = 3$). **D,** Representative images of cellular morphologies under 2D and 3D collagen culture conditions. Scale bar, 50 μm. **E,** Cell areas under 2D or 3D collagen culture conditions ($n = 50$). **F,** Roundness index under the 2D or 3D collagen culture conditions ($n = 50$). **G,** Representative confocal images of control cells with membrane blebs under the 3D collagen culture condition. Phalloidin stain was performed. White arrow heads indicate membrane blebs. Scale bar, 10 μm. **H–I,** Representative images (**G**) and quantification (**H**) of gel contraction rate. The yellow dashed line indicates the shape of the collagen gels, and the red dashed line indicates the well of the culture plate ($n = 3$). Graphs show mean ± SD. Dunnett test: *, $P < 0.05$; **, $P < 0.01$. Ctrl: control, KO#1: podoplanin-KO cell line 1, KO#2: podoplanin-KO cell line 2.

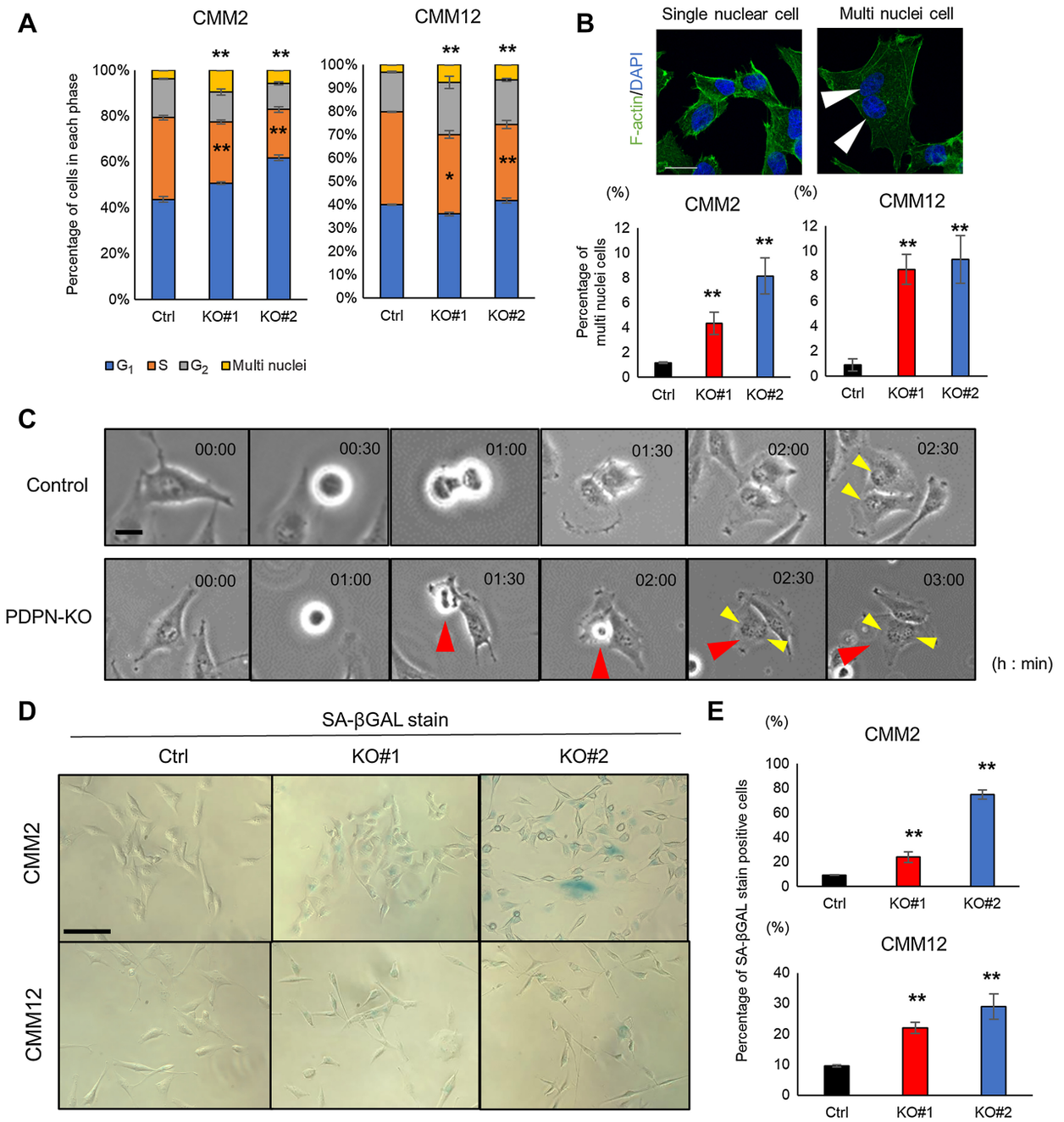

Figure 4.

Loss of podoplanin leads to cell-cycle arrest and cellular senescence. **A,** Cell-cycle analysis ($n = 3$). **B,** Phalloidin- and DAPI-stained CMM2 cells (top) and the percentage of multi nuclei cells (bottom; $n = 3$). White arrowheads indicate nuclei. Scale bar: 50 μm. **C,** Time-lapse images during the proliferation of control (CMM2) and PDPN-KO (KO#2 of CMM2) cells. Red arrowheads show cytokinesis failure cells among PDPN-KO cells, and yellow arrowheads show nuclei in control and PDPN-KO cells. Scale bar, 10 μm. **D,** Representative images of SA-β-GAL staining. Scale bar, 50 μm. **E,** Percentage of SA-βGAL stain-positive cells ($n = 3$). Graphs show mean ± SD. Dunnett test: *, $P < 0.05$; **, $P < 0.01$. Ctrl: control, KO#1: PDPN-KO cell line 1, KO#2: PDPN-KO cell line 2.

mucosal melanoma cells showed similar effects as those found in PDPN-KO cells, and restoring podoplanin expression in the PDPN-KO cells showed recovery of those characteristics, suggesting that podoplanin regulated the features of amoeboid invasion via ROCK-MLC2 signaling in canine mucosal melanoma cells.

Podoplanin promotes amoeboid invasion features in xenografted mouse models and clinical cases

To determine whether abrogation of podoplanin suppresses amoeboid invasion in canine mucosal melanoma cells *in vivo*, we generated xenograft murine xenograft models that exhibited similar podoplanin

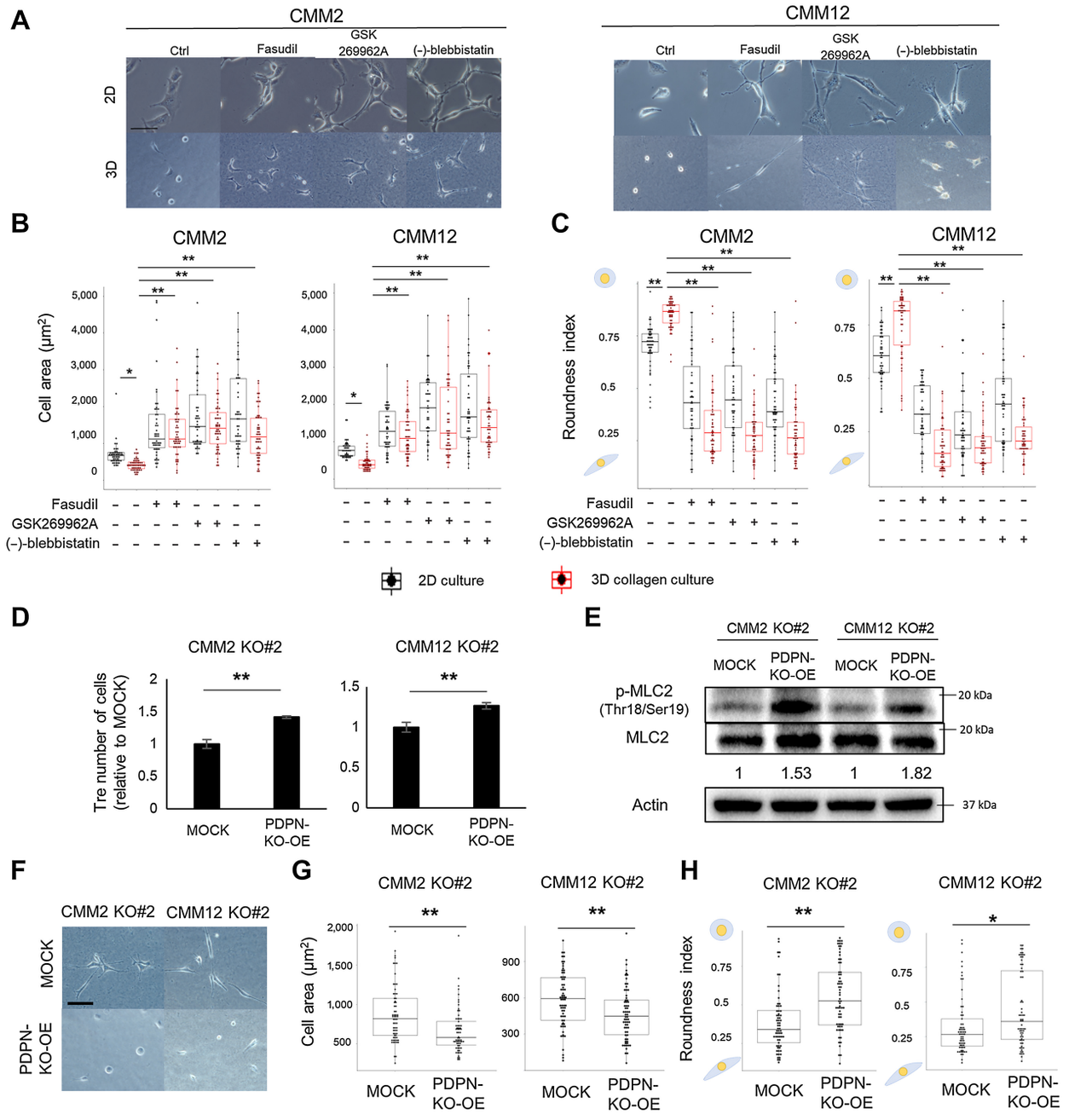

Figure 5.

Podoplanin-ROCK-MLC2 signaling is the regulator of amoeboid invasion of canine mucosal melanoma cells. **A,** Representative images of cellular morphologies under the 2D and 3D collagen culture conditions at 24 hours after inhibitors treatment. Scale bar, 50 μm. **B,** Cell areas at 24 hours after inhibitors treatment ($n = 50$). Dunnett test. **C,** Roundness index of cells at 24 hours after inhibitors treatment ($n = 50$). Dunnett test. **D,** Number of live cells of MOCK control and podoplanin overexpressed PDPN-KO (PDPN-KO-OE) cells ($n = 3$). The number of cells were counted at 72 hours after cell seeding. **E,** Immunoblots of p-MLC2. Levels of phosphor-protein expression were calculated after correction to total levels of the relevant protein expression and are indicated under the immunoblot images of each total protein. **F,** Representative images of cellular morphologies of MOCK control and PDPN-KO-OE cells under 3D collagen culture conditions. Scale bar: 50 μm. **G,** Cell areas of MOCK control and PDPN-KO-OE cells under 3D collagen culture conditions ($n = 65$). Box limits show the 25th and 75th percentiles, the horizontal line represents the median, and dotted plots show the scores of each cell. Dunnett test. **H,** Roundness index of MOCK control and PDPN-KO-OE cells under 3D collagen culture conditions ($n = 65$). Box limits show the 25th and 75th percentiles, the horizontal line represents the median, and dotted plots show the scores of each cell. Dunnett test. *, $P < 0.05$; **, $P < 0.01$.

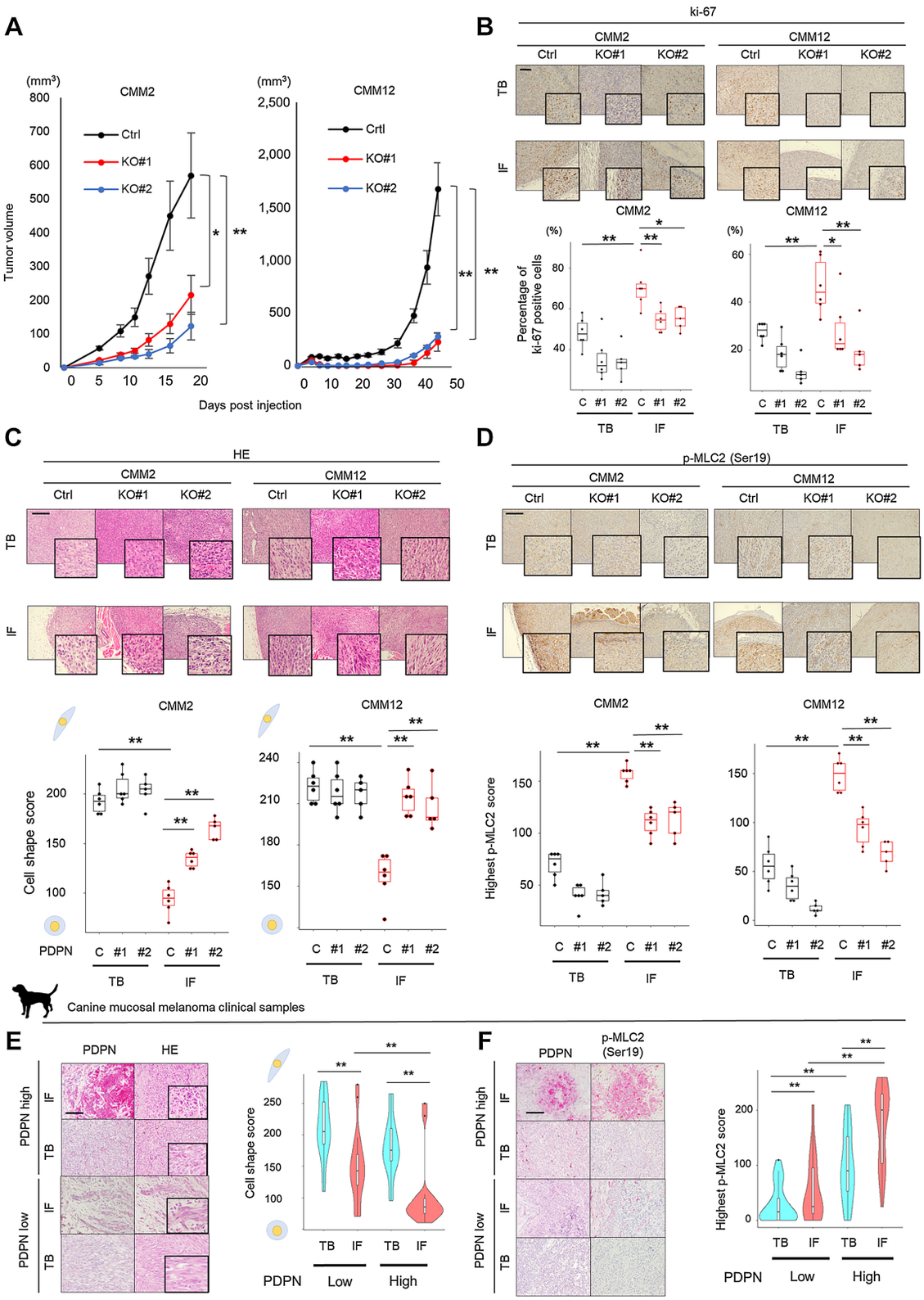

expression patterns to those of canine mucosal melanoma clinical samples (Supplementary Fig. S8A). Tumor growth was significantly suppressed by PDPN-KO (**Fig. 6A**). These results indicated that podoplanin promoted proliferative and aggressive amoeboid invasion in xenografted tumor tissues at the IFs.

To assess whether these observations were recapitulated in clinical samples, we conducted IHC analysis. In control tumors, the percentage of ki-67–expressing cells at the IFs was significantly higher and, that of p21-expressing cells at the IFs was significantly lower, compared with that of the TBs (**Fig. 6B**; Supplementary Fig. S8B). Cell roundness and phosphor-MLC2 expression levels at the IFs were significantly higher than those of the TBs in control tumors (**Fig. 6C** and **D**). Notably, the percentage of ki-67, p21-expressing cells, cell roundness, and phospho-MLC2 expression levels at the IFs of PDPN-KO tumors were reversed to levels similar to those in the TBs of PDPN-KO tumors (**Fig. 6B–D**; Supplementary Fig. S8B). The IFs of canine mucosal melanoma enriched rounded tumor cells compared with the TBs, and the number of rounded cells in the IFs was associated with podoplanin expression levels in the IFs (**Fig. 6E**). Phospho-MLC2 expression levels at the IFs were higher than the TBs, and phosphor-MLC2 expression levels in the IFs were associated with podoplanin expression levels in the IFs (**Fig. 6F**). These data suggested that podoplanin induced aggressive amoeboid invasion in the IFs of canine mucosal melanoma, which was linked to unfavorable outcomes in dogs.

To explore the relationship between podoplanin and distant colonization of canine mucosal melanoma cells, an *in vivo* lung metastasis assay was performed, and the number of lung metastatic foci was significantly reduced by PDPN-KO (Supplementary Fig. S9A and S9B). This result suggests that PDPN promotes distant colonization during the late stage of tumor metastasis.

Canine and human mucosal melanomas with high podoplanin expression are enriched with gene signatures associated with amoeboid invasion

We analyzed three cohorts of public datasets for canine oral mucosal melanoma (44–46). The expression of the podoplanin gene level was significantly higher in tumor tissues than in normal control tissues (Supplementary Fig. S10A). GO term enrichment analysis showed that tumors that exhibited high podoplanin expression were enriched in genes related to ROCK/cytoskeleton (Supplementary Fig. S10B). GSEA displayed that tumors with high PDPN expression were enriched in gene signatures relevant to amoeboid invasion, proliferation, migration, and invasion (Supplementary Figs. S10C, S10D, and S11). These findings suggest that podoplanin-dependent induction of proliferative and aggressive amoeboid invasion is a common characteristic of canine mucosal melanoma cells expressing podoplanin.

To assess the applicability of our discoveries from canine to human mucosal melanoma, we investigated three human mucosal melanoma public datasets (47, 48). The expression of the podoplanin gene level was significantly higher in human mucosal melanoma tissues than in normal control tissues (Supplementary Fig. S12A). Survival analysis of patients with stage 3 or 4 mucosal melanoma ($n = 11$) showed that patients with high podoplanin-expressing tumors had significantly shorter PFS and OS than those with low podoplanin-expressing tumors (**Fig. 7A**). Tumors with high podoplanin expression were enriched in of ROCK/cytoskeleton-related and amoeboid invasion-related gene signatures (**Fig. 7B** and **C**). Tumors with high podoplanin expression showed enhanced gene expression of collagens associated with amoeboid invasion *(COL1A1, COL1A2, COL4A1*, and *COL4A2*; Supplementary Fig. S12B). Tumors with high podoplanin expression had enriched gene signatures related to proliferation, migration, and invasion (**Fig. 7D**; Supplementary Fig. S12C). Moreover, the upregulation pattern of common mesenchymal amoeboid transition-related genes was similar between human and canine mucosal melanomas (**Fig. 7E**). These findings suggest that podoplanin promotes amoeboid invasion in human mucosal melanoma through mechanisms similar to those observed in canine mucosal melanoma.

Discussion

Podoplanin has been reported to drive amoeboid invasion in murine cutaneous melanoma cells (32); however, that relationship in canine and human melanoma had not been revealed. Especially in canine and human mucosal melanoma, the relationship between podoplanin and tumor malignancies had not been comprehensively understood. In this study, we demonstrated that podoplanin overexpressed in the tumor IFs was associated with poor prognosis in dogs with mucosal melanoma and that podoplanin regulated features of amoeboid invasion in canine mucosal melanoma cells via podoplanin-ROCK–MLC2 signaling. Podoplanin expression was also related to the enrichment of amoeboid invasion-related gene signatures in canine and human mucosal melanoma tissues. These findings suggest that podoplanin drives amoeboid invasion to acquire highly metastatic features in canine and human mucosal melanoma.

Canine mucosal melanoma is one of the most common oral malignancies in dogs and is a highly aggressive tumor that can metastasize during the early stages of the disease (8, 10). The 1-year survival rate of dogs with mucosal melanoma is less than 35% owing to a high metastatic rate of more than 70% (8, 10). In this study, we demonstrated that podoplanin overexpressed in the IFs of canine mucosal melanoma was related to reduced PFS and OS rates, indicating that podoplanin overexpressed in the IFs is a key molecule in canine mucosal melanoma metastasis. We showed that podoplanin depletion in canine mucosal melanoma cells downregulated the activation of ERM, RhoA, and ROCK-MLC2. Moreover, podoplanin depletion and ROCK inhibition suppressed amoeboid invasion features in canine mucosal melanoma cells, and restoring podoplanin expression reactivated ROCK-MLC2 signaling in podoplanin-KO cells. Podoplanin directly binds to ERM protein to activate RhoA (20), and ROCK is a major effector molecule of the activated RhoA. Amoeboid invasion has been reported to be induced by ROCK-MLC2 signaling activation (27–31). Therefore, podoplanin would promote amoeboid invasion by activating ERM-RhoA–ROCK-MLC2 signaling. During the early step of tumor metastasis, human cutaneous

Figure 6.

Podoplanin promotes amoeboid invasion features in xenografted mouse models and clinical cases. **A,** Tumor growth curves xenografted in immunodeficient mice ($n = 5$–7). Graphs show the mean ± SEM. Dunnett test. **B–D,** Representative images of the TBs and IFs of control and podoplanin-KO tumors (top) and quantification (bottom) of the percentage of ki-67–positive cells (**B**), melanoma cell shape score (**C**), and p-MLC2 IHC score (**D**) of xenografted tissues from **A** ($n = 5$–6). Ki-67 and p-MLC2 were stained with DAB. Scale bar: 200 μm. Dunnett test. **E** and **F,** Representative images of canine mucosal melanoma tissues showing podoplanin expression, H&E staining, and p-MLC2 expression in the TBs and IFs (left) and quantification (right) of melanoma cell shape score (**E**) and p-MLC2 IHC score (**F**) in the TBs and IFs of canine mucosal melanoma clinical samples from **Fig. 1** ($n = 40$ and 34, respectively). High or low podoplanin expression samples were divided by the median podoplanin expression score in the IFs. Podoplanin and p-MLC2 were stained with alkaline phosphatase, and podoplanin- and pMLC2-positive cells were stained red. Scale bar, 100 μm. One-way ANOVA with Tukey–Kramer test: *, $P < 0.05$; **, $P < 0.01$. **C,** Control, #1: PDPN-KO cell line 1, #2: PDPN-KO cell line 2.

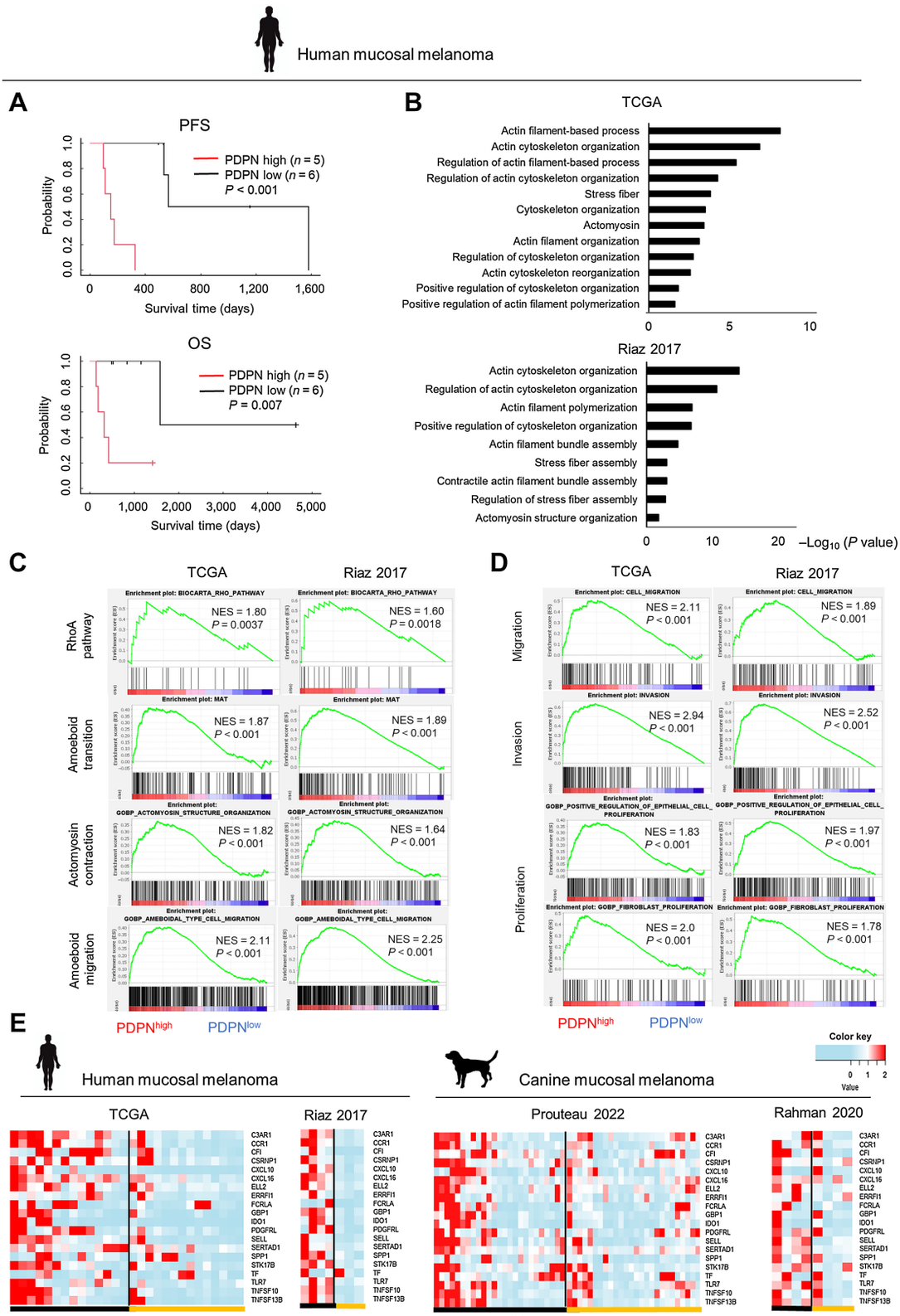

melanoma cells change their cellular morphology into the aggressive amoeboid mode by activating ROCK-MLC2 signaling to invade adjacent tissues (27–31). Amoeboid invasion is a faster, more efficient, and less energy-consuming mode than the mesenchymal mode, potentiating the ability of cancer cells to migrate and invade the extracellular environment (49). In the late stage of metastasis, amoeboid invading human cutaneous melanoma cells promote distant colonization by disrupting endothelial junctions and increasing endothelial cell permeability via secretion of IL1α and activation of NF-κB, promoting extravasation and metastasis colonization (27). In this study, we obtained similar results that abrogation of podoplanin-ROCK–MLC2 signaling in canine mucosal melanoma cells suppressed amoeboid invasion features in the IFs of primary tumor tissues and tumor colonization in distant organs. Overall, podoplanin expressed in the IFs of canine mucosal melanoma cells would be a major promoter of the series of their metastatic process.

Amoeboid-invading human cutaneous melanoma cells have a high proliferative capacity (29). In our study, podoplanin deletion and ROCK-MLC2 signaling inhibitions suppressed cell proliferation, suggesting that podoplanin promoted the proliferation of amoeboid invading cells. In podoplanin-KO cells, S-phase cell-cycle entry was inhibited, and a high expression of CDKi mRNA was observed. Tumor cells often downregulate CDKi expression to promote rapid cell proliferation because CDKi negatively regulates cell-cycle progression (50, 51). RhoA activation in tumor cells was reported as a possible mechanism of CDKi suppression. A previous report showed that RhoA suppression in human gastric cancer cells induced p21 and p27 upregulation and decreased the number of cells in S-phase cell-cycle (52). Therefore, our findings suggest that podoplanin would promote S-phase cell-cycle entry in canine mucosal melanoma cells by suppressing CDKi expression probably through RhoA activation and that podoplanin promotes the proliferation of amoeboid invading cells in the canine mucosal melanoma IFs.

Furthermore, we found that podoplanin depletion and inhibition of ROCK-MLC2 induced cellular senescence and cytokinesis failure in canine mucosal melanoma cells. Cellular senescence is a state of permanent cell-cycle arrest that occurs in response to stress; therefore, cellular senescence could be a barrier that tumor cells need to evade to maintain an aberrant proliferation (53, 54). Cytokinesis failure has been reported to induce cellular senescence in human colon cancer cells and rat embryo fibroblasts (55, 56). In addition, it was reported that RhoA and MLC2 inhibition led to cytokinesis failure in murine embryo fibroblasts; hence, RhoA–ROCK-MLC2 signaling activation is involved in cytokinesis progression (57, 58). Overall, cytokinesis failure caused by podoplanin depletion would induce cellular senescence in canine mucosal melanoma cells. Although it was reported that cytokinesis failure induced cellular senescence, the detailed mechanism has yet to be comprehensively described. Cytokinesis failure was reported to generate lagging chromosomes and micronuclei leading to DNA damage response that induces cellular senescence (59). A previous report showed that inhibition of ROCK induced DNA damage in human melanoma cells (60). Other report suggested that cytokinesis failure in RPE-1 cells prevented cell proliferation by activating the large tumor suppressor kinase 2 (LATS2), which inactivated YAP and stabilized p53 (61). Overall, our findings suggest that podoplanin-RhoA–ROCK-MLC2 signaling in amoeboid invading canine mucosal melanoma cells supports the escape from cellular senescence by preventing cytokinesis failure, caused by high proliferative activity, and further research is required to reveal the detailed mechanism.

A previous study indicated that PDPN senses a stiffness of external environment and regulates fibroblast proliferation (42). We found that the proliferation of control cells increased on the noncollagen dish compared to the collagen thick-layer dish, and the changes depended on the PDPN expression in canine mucosal melanoma cells. As tumor stiffness increased from the tumor core region to the tumor periphery (62), podoplanin might have sensed a stiffer microenvironment of canine mucosal melanoma IFs and promoted the proliferation of amoeboid-invading cells in the IFs.

Human mucosal melanoma is a rare and the most aggressive subtype, and it is difficult for surgery to achieve radical excision, owing to the lentiginous growth pattern, multifocal nature, and high metastasis rate of approximately 80% (1). Although adjuvant radiotherapy is performed for the local control of human mucosal melanoma, it could not reduce the risk of distant metastasis and prolong patients' survival (63, 64). In addition, patients with mucosal melanoma show lower response rates to immune checkpoint blockades than those with cutaneous melanoma (23 vs. 40.9%; ref. 65). Therefore, it is crucial to understand the molecular mechanism of human mucosal melanoma metastasis. Our study revealed that high podoplanin expression in human mucosal melanoma is associated with poor prognosis and the enrichment of amoeboid invasion-related gene signatures, as observed in canine mucosal melanoma. Furthermore, we found that the upregulation pattern of mesenchymal amoeboid transition-related genes was similar between podoplanin high-expressing human and canine mucosal melanoma tissues. These findings suggest that podoplanin drives amoeboid invasion and metastasis in human mucosal melanoma through similar mechanisms as those acting in canine mucosal melanoma. Thus, naturally occurring canine mucosal melanoma could be a novel research model for podoplanin expressing human mucosal melanoma.

We showed that podoplanin was overexpressed in the IFs of canine mucosal melanoma tissues; however, the induction mechanism of podoplanin remains unclear. A previous study showed that podoplanin expression is induced by inflammatory cytokines such as IFNγ, TGFβ, and/or tumor necrosis factor-α in human SCC cells (66). Tumor IFs are located adjacent tumor stromal regions enriched with inflammatory immune cells; thus, tumor cells in the TFs could be strongly exposed to inflammatory cytokines released from inflammatory immune cells in stromal regions (67). Therefore, inflammatory cytokine may induce podoplanin expression on canine melanoma cells in the TIF, leading to aggressive amoeboid invasion.

Our study opens the possibility that podoplanin plays a crucial role in amoeboid invasion and metastasis of canine and human mucosal melanoma. podoplanin could be used as a biomarker and a therapeutic target for the restriction of amoeboid invasion and metastatic dissemination in canine and human mucosal melanoma.

Figure 7.

Human mucosal melanomas with podoplanin high expression demonstrates enrichment of gene signatures associated with amoeboid invasion. **A,** Kaplan–Meier survival curves for PFS and OS of human patients with stages 3 or 4 mucosal melanoma above or below the median podoplanin gene expression from The Cancer Genome Atlas (TCGA) dataset ($n = 11$). Log-rank test. **B,** Enriched GO terms in high podoplanin-expressing human mucosal melanoma tissues. The *x*-axis indicates the $-\log_{10} P$ value. **C** and **D,** GSEA plots showing enriched gene signatures in high podoplanin expressing human mucosal melanoma tissues. NES: normalized enrichment score. **E,** Heat maps demonstrating the relative expression of mesenchymal amoeboid transition-related genes in human and canine mucosal melanoma tissues. The color key indicates the fold change (FC) in gene expression from the average expression.

Authors' Disclosures

D. Kato reports grants from JSPS KAKENHI during the conduct of the study. Y. Takahashi reports grants from JSPS KAKENHI during the conduct of the study. R. Nishimura reports grants from JSPS KAKENHI during the conduct of the study. No disclosures were reported by the other authors.

Authors' Contributions

M. Shinada: Data curation, formal analysis, investigation, visualization, writing-original draft, writing–review and editing. **D. Kato:** Conceptualization, data curation, formal analysis, supervision, funding acquisition, validation, project administration, writing–review and editing. **T. Motegi:** Resources, software, formal analysis, bioinformatics analysis. **M. Tsuboi:** Resources, visualization, assist in pathological evaluation. **N. Ikeda:** Data curation. **S. Aoki:** Data curation, formal analysis. **T. Iguchi:** Data curation, formal analysis. **T. Li:** Data curation, formal analysis. **Y. Kodera:** Data curation, formal analysis. **R. Ota:** Data curation, formal analysis. **Y. Hashimoto:** Resources. **Y. Takahashi:** Resources, funding acquisition. **J. Chambers:** Resources, provision of paraffin samples. **K. Uchida:** Resources. **Y. Kato:** Resources, funding acquisition, provision of antibodies. **R. Nishimura:** Conceptualization, supervision, funding acquisition, project administration. **T. Nakagawa:** Conceptualization, supervision, project administration.

Acknowledgments

We thank all the staff of the Veterinary Medical Center of the University of Tokyo, the Laboratory of Veterinary Pathology who processed the samples, and the dog owners. This work was supported by JSPS KAKENHI (Grant Numbers 19K22361, 20H03141, and 21K20614) and in part by Japan Agency for Medical Research and Development (AMED; grant Numbers JP22ama121008 and JP22am0401013).

The publication costs of this article were defrayed in part by the payment of publication fees. Therefore, and solely to indicate this fact, this article is hereby marked "advertisement" in accordance with 18 USC section 1734.

Note

Supplementary data for this article are available at Molecular Cancer Research Online (http://mcr.aacrjournals.org/).

Received November 19, 2022; revised April 9, 2023; accepted July 13, 2023; published first July 26, 2023.

References

1. Ma Y, Xia R, Ma X, Judson-Torres RL, Zeng H. Mucosal melanoma: pathological evolution, pathway dependency and targeted therapy. Front Oncol 2021;11:702287.
2. Chae YS, Lee JY, Lee JW, Park JY, Kim SM, Lee JH. Survival of oral mucosal melanoma according to treatment, tumour resection margin, and metastases. Br J Oral Maxillofac Surg 2020;58:1097–102.
3. Mihajlovic M, Vlajkovic S, Jovanovic P, Stefanovic V. Primary mucosal melanomas: a comprehensive review. Int J Clin Exp Pathol 2012;5:739–53.
4. Minhahn H, Geunlee K, Choi W, Cheong SH, Myung KB, Hahn HJ. An updated review of mucosal melanoma: survival meta-analysis. Mol Clin Oncol 2019;11:116–26.
5. Baderca F, Vincze D, Balica N, Solovan C. Mucosal melanomas in the elderly: challenging cases and review of the literature. Clin Interv Aging 2014;9:929–37.
6. Carbó-Bagué A, Rubió-Casadevall J, Puigdemont M, Sanvisens A, Oliveras G, Coll M, et al. Epidemiology and molecular profile of mucosal melanoma: a population-based study in southern Europe. Cancers (Basel) 2022;14:780.
7. Plavc G, But-Hadžić J, Aničin A, Lanišnik B, Didanović V, Strojan P. Mucosal melanoma of the head and neck: a population-based study from Slovenia, 1985–2013. Radiat Oncol 2016;11:137.
8. Hernandez B, Adissu HA, Wei BR, Michael HT, Merlino G, Mark Simpson R. Naturally occurring canine melanoma as a predictive comparative oncology model for human mucosal and other triple wild-type melanomas. Int J Mol Sci 2018;19:394.
9. Nishiya AT, Massoco CO, Felizzola CR, Perlmann E, Batschinski K, Tedardi MV, et al. Comparative aspects of canine melanoma. Vet Sci 2016;3:7.
10. Williams LE, Packer RA. Association between lymph node size and metastasis in dogs with oral malignant melanoma: 100 cases (1987–2001). J Am Vet Med Assoc 2003;222:1234–36.
11. Hendricks WPD, Zismann V, Sivaprakasam K, Legendre C, Poorman K, Tembe W, et al. PTPRJ mutations and dysregulated pathways identified in canine malignant melanoma by integrated comparative genomic analysis. PLoS Genet 2018;14:e1007589.
12. Prouteau A, André C. Canine melanomas as models for human melanomas: clinical, histological, and genetic comparison. Genes (Basel) 2019;10:501.
13. Wong K, van der Weyden L, Schott CR, Foote A, Constantino-Casas F, Smith S, et al. Cross-species genomic landscape comparison of human mucosal melanoma with canine oral and equine melanoma. Nat Commun 2019;10:353.
14. LeBlanc AK, Mazcko CN. Improving human cancer therapy through the evaluation of pet dogs. Nat Rev Cancer 2020;20:727–42.
15. Paoloni M, Khanna C. Translation of new cancer treatments from pet dogs to humans. Nat Rev Cancer 2008;8:147–56.
16. Hayakawa Y, Kawada M, Nishikawa H, Ochiya T, Saya H, Seimiya H, et al. Report on the use of non-clinical studies in the regulatory evaluation of oncology drugs. Cancer Sci 2016;107:189–202.
17. Kamoto S, Shinada M, Kato D, Yoshimoto S, Ikeda N, Tsuboi M, et al. Phase I/II clinical trial of the anti-podoplanin monoclonal antibody therapy in dogs with malignant melanoma. Cells 2020;9:2529.
18. Shinada M, Kato D, Kamoto S, Yoshimoto S, Tsuboi M, Yoshitake R, et al. PDPN is expressed in various types of canine tumors and its silencing induces apoptosis and cell cycle arrest in canine malignant melanoma. Cells 2020;9:1136.
19. Takeuchi S, Fukuda K, Yamada T, Arai S, Takagi S, Ishii G, et al. Podoplanin promotes progression of malignant pleural mesothelioma by regulating motility and focus formation. Cancer Sci 2017;108:696–703.
20. Martín-Villar E, Megías D, Castel S, Yurrita MM, Vilaró S, Quintanilla M. Podoplanin binds ERM proteins to activate RhoA and promote epithelial-mesenchymal transition. J Cell Sci 2006;119:4541–53.
21. Quintanilla M, Montero LM, Renart J, Villar EM. Podoplanin in inflammation and cancer. Int J Mol Sci 2019;20:707.
22. Ugorski M, Dziegiel P, Suchanski J. Podoplanin-a small glycoprotein with many faces. Am J Cancer Res 2016;6:370–86.
23. Hamada M, Ebihara Y, Nagata K, Yano M, Kogashiwa Y, Nakahira M, et al. Podoplanin is an efficient predictor of neck lymph node metastasis in tongue squamous cell carcinoma with low tumor budding grade. Oncol Lett 2020;19:2602–08.
24. Kim HY, Rha KS, Shim GA, Kim JH, Kim JM, Huang SM, et al. Podoplanin is involved in the prognosis of head and neck squamous cell carcinoma through interaction with VEGF-C. Oncol Rep 2015;34:833–42.
25. Ochoa-Alvarez JA, Krishnan H, Shen Y, Acharya NK, Han M, McNulty DE, et al. Plant lectin can target receptors containing sialic acid, exemplified by podoplanin, to inhibit transformed cell growth and migration. PLoS One 2012;7:e41845.
26. Xu M, Wang X, Pan Y, Zhao X, Yan B, Ruanet C, et al. Blocking podoplanin suppresses growth and pulmonary metastasis of human malignant melanoma. BMC Cancer 2019;19:599.
27. Georgouli M, Herraiz C, Crosas-Molist E, Fanshawe B, Maiques O, Perdrix A, et al. Regional activation of myosin II in cancer cells drives tumor progression via a secretory cross-talk with the immune microenvironment. Cell 2019;176:757–74.
28. Graziani V, Rodriguez-Hernandez I, Maiques O, Sanz-Moreno V. The amoeboid state as part of the epithelial-to-mesenchymal transition programme. Trends Cell Biol 2022;32:228–42.
29. Rodriguez-Hernandez I, Maiques O, Kohlhammer L, Cantelli G, Perdrix-Rosell A, Monger J, et al. WNT11-FZD7-DAAM1 signalling supports tumour initiating abilities and melanoma amoeboid invasion. Nat Commun 2020;11:5315.
30. Sahai E, Marshall CJ. Differing modes of tumour cell invasion have distinct requirements for Rho/ROCK signalling and extracellular proteolysis. Nat Cell Biol 2003;5:711–19.
31. Sanz-Moreno V, Gaggioli C, Yeo M, Albrengues J, Wallberg F, Viros A, et al. ROCK and JAK1 signaling cooperate to control actomyosin contractility in tumor cells and stroma. Cancer Cell 2011;20:229–45.

32. de Winde CM, George SL, Crosas-Molist E, Hari-Gupta Y, Arp AB, Benjamin AC, et al. Podoplanin drives dedifferentiation and amoeboid invasion of melanoma. iScience 2021;24:102976.
33. Igase M, Shibutani S, Kurogouchi Y, Fujiki N, Hwang CC, Coffey M, et al. Combination therapy with reovirus and ATM inhibitor enhances cell death and virus replication in canine melanoma. Mol Ther Oncolytics 2019;28:49–59.
34. Ohashi E, Hong SH, Takahashi T, Nakagawa T, Mochizuki M, Nishimura R, et al. Effect of retinoids on growth inhibition of two canine melanoma cell lines. J Vet Med Sci 2001;63:83–6.
35. Schneider CA, Rasband WS, Eliceiri KW. NIH image to imageJ: 25 years of image analysis. Nat Methods 2012;9:671–75.
36. Chen S, Zhou Y, Chen Y, Gu J. Fastp: an ultra-fast all-in-one FASTQ preprocessor. Bioinformatics 2018;34:i884–90.
37. Maeda S, Motegi T, Iio A, Kaji K, Goto-Koshino Y, Eto S, et al. Anti-CCR4 treatment depletes regulatory T cells and leads to clinical activity in a canine model of advanced prostate cancer. J Immunother Cancer 2022;10:e003731.
38. Subramanian A, Tamayo P, Mootha VK, Mukherjee S, Ebert BL, Gillette MA, et al. Gene set enrichment analysis: a knowledge-based approach for interpreting genome-wide expression profiles. Proc Natl Acad Sci USA 2005;102:15545–50.
39. Verfaillie A, Imrichova H, Atak ZK, Dewaele M, Rambow F, Hulselmans G, et al. Decoding the regulatory landscape of melanoma reveals TEADS as regulators of the invasive cell state. Nat Commun 2015;6:6683.
40. Emad A, Ray T, Jensen TW, Parat M, Natrajan R, Sinha S, et al. Superior breast cancer metastasis risk stratification using an epithelial-mesenchymal-amoeboid transition gene signature. Breast Cancer Res 2020;22:74.
41. Tsoi MF, Thaiwong T, Smedley RC, Noland E, Kiupel M. Quantitative expression of TYR, CD34, and CALD1 discriminates between canine oral malignant melanomas and soft tissue sarcomas. Front Vet Sci 2021;8:701457.
42. Horsnell HL, Tetley RJ, De Belly H, Makris S, Millward LJ, Benjamin AC, et al. Lymph node homeostasis and adaptation to immune challenge resolved by fibroblast network mechanics. Nat Immunol 2022;23:1169–82.
43. Normand G, King RW. Understanding cytokinesis failure. Adv Exp Med Biol 2010;675:27–55.
44. Bowlt Blacklock KL, Birand Z, Selmic LE, Nelissen P, Murphy S, Blackwood L, et al. Genome-wide analysis of canine oral malignant melanoma metastasis-associated gene expression. Sci Rep 2019;9:6511.
45. Prouteau A, Mottier S, Primot A, Cadieu E, Bachelot L, Botherel N, et al. Canine oral melanoma genomic and transcriptomic study defines two molecular subgroups with different therapeutical targets. Cancers (Basel) 2022;14:276.
46. Rahman MM, Lai YC, Husna AA, Chen HW, Tanaka Y, Kawaguchi H, et al. Transcriptome analysis of dog oral melanoma and its oncogenic analogy with human melanoma. Oncol Rep 2020;43:16–30.
47. Wolf J, Auw-Haedrich C, Schlecht A, Boneva S, Mittelviefhaus H, Lapp T, et al. Transcriptional characterization of conjunctival melanoma identifies the cellular tumor microenvironment and prognostic gene signatures. Sci Rep 2020;10:17022.
48. Riaz N, Havel JJ, Makarov V, Desrichard A, Urba WJ, Sims JS, et al. Tumor and microenvironment evolution during immunotherapy with nivolumab. Cell 2017;171:934–49.
49. Hecht I, Bar-El Y, Balmer F, Natan S, Tsarfaty I, Schweitzer F, et al. Tumor invasion optimization by mesenchymal-amoeboid heterogeneity. Sci Rep 2015;5:10622.
50. Abukhdeir AM, Park BH. P21 and P27: roles in carcinogenesis and drug resistance. Expert Rev Mol Med 2008;10:e19.
51. Zhang M, Zhang L, Hei R, Li X, Cai H, Wu X, et al. CDK inhibitors in cancer therapy, an overview of recent development. Am J Cancer Res 2021;11:1913–35.
52. Zhang S, Tang Q, Xu F, Xue Y, Zhen Z, Deng Y, et al. RhoA regulates G1-S progression of gastric cancer cells by modulation of multiple INK4 family tumor suppressors. Mol Cancer Res 2009;7:570–80.
53. Ou HL, Hoffmann R, González-López C, Doherty GJ, Korkola JE, Muñoz-Espín D. Cellular senescence in cancer: from mechanisms to detection. Mol Oncol 2021;15:2634–71.
54. Wang L, Lankhorst L, Bernards R. Exploiting senescence for the treatment of cancer. Nat Rev Cancer 2022;22:340–55.
55. Panopoulos A, Pacios-Bras C, Choi J, Yenjerla M, Sussman MA, Fotedar R, et al. Failure of cell cleavage induces senescence in tetraploid primary cells. Mol Biol Cell 2014;25:3105–118.
56. Zhang Z, Aung KM, Uhlin BE, Wai SN. Reversible senescence of human colon cancer cells after blockage of mitosis/cytokinesis caused by the CNF1 cyclomodulin from Escherichia coli. Sci Rep 2018;8:17780.
57. Duan X, Liu J, Zhu CC, Wang QC, Cui XS, Kim NH, et al. RhoA-mediated MLC2 regulates actin dynamics for cytokinesis in meiosis. Cell Cycle 2016;15:471–77.
58. Konstantinidis DG, Giger KM, Risinger M, Risinger M, Pushkaran S, Zhou P, et al. Cytokinesis failure in RhoA-deficient mouse erythroblasts involves actomyosin and midbody dysregulation and triggers p53 activation. Blood 2015;126:1473–82.
59. Hayashi MT, Karlseder J. DNA damage associated with mitosis and cytokinesis failure. Oncogene 2013;32:4593–601.
60. Herraiz C, Calvo F, Pandya P, Cantelli G, Rodriguez-Hernandez I, Orgaz JL, et al. Reactivation of p53 by a cytoskeletal sensor to control the balance between DNA damage and tumor dissemination. J Natl Cancer Inst 2015;108:djv289.
61. Ganem NJ, Cornils H, Chiu SY, O'Rourke KP, Arnaud J, Yimlamai D, et al. Cytokinesis failure triggers hippo tumor suppressor pathway activation. Cell 2014;158:833–48.
62. Liu C, Li M, Dong ZX, Jiang D, Li X, Lin S, et al. Heterogeneous microenvironmental stiffness regulates pro-metastatic functions of breast cancer cells. Acta Biomater 2021;131:326–40.
63. Li W, Yu Y, Wang H, Yan A, Jiang X. Evaluation of the prognostic impact of postoperative adjuvant radiotherapy on head and neck mucosal melanoma: a meta-analysis. BMC Cancer 2015;15:758.
64. Lu Z, Zhou Y, Nie G, Miao B, Lu Y, Chen T. Prognostic nomograms for predicting overall survival and cancer-specific survival in patients with head and neck mucosal melanoma. Int J Gen Med 2022;15:2759–71.
65. Yentz S, Lao CD. Immunotherapy for mucosal melanoma. Ann Transl Med 2019;7:S118.
66. Kunita A, Baeriswyl V, Meda C, Cabuy E, Takeshita K, Giraudo E, et al. Inflammatory cytokines induce podoplanin expression at the tumor invasive front. Am J Pathol 2018;188:1276–88.
67. Seager RJ, Hajal C, Spill F, Kamm RD, Zaman MH. Dynamic interplay between tumour, stroma and immune system can drive or prevent tumour progression. Converg Sci Phys Oncol 2017;3:034002.